

Presentation of Calibration Coefficient to Measure Non-Uniform Residual Stresses by the Integral Ring-core Method

M.A. Moazam, M. Honarpisheh*

Mechanical Engineering Department, University of Kashan, Kashan, Iran.

Article info

Article history:

Received 23 September 2018

Received in revised form

29 January 2019

Accepted 03 February 2019

Keywords:

Residual stress

Non-uniform

Ring-core

Calibration coefficient

Integral

Incremental

Abstract

The aim of this paper is to compare incremental and integral techniques in non-uniform residual stress measurement by the ring-core method and to present a procedure to determine the calibration coefficients of the integral technique. The mathematical basis of the integral technique for use in the ring-core method is explained. To determine the calibration coefficients of the integral technique a 3D FE model was introduced and the calibration coefficients are also presented in separate tables. The FE analysis of the pure bending and ring-core method were used to show the effectiveness of the presented coefficients and compare the integral and incremental techniques. The results indicated that the calculated non-uniform residual stresses by the integral technique were closer to the real values in comparison with the incremental method. Moreover, it was observed that the accuracy of the results decreased by increasing the depth of the groove.

Nomenclature

| | | | |
|--------------------------------|--|--------------------------------|--|
| $\frac{d\varepsilon_a(z)}{dz}$ | The released strains due to the depth increment in direction of the strain gages (a) | $\frac{d\varepsilon_b(z)}{dz}$ | The released strains due to the depth increment in direction of the strain gages (b) |
| $\frac{d\varepsilon_c(z)}{dz}$ | The released strains due to the depth increment in direction of the strain gages (c) | α_k | Angle between the maximum principal residual stress and measuring direction K |
| $K_1(z)$ | Calibration constant | $K_2(z)$ | Calibration constant |
| $\sigma_a(z)$ | Residual stress in direction of the strain gages (a) | $\sigma_b(z)$ | Residual stress in direction of the strain gages (b) |
| $\sigma_c(z)$ | Residual stress in direction of the strain gages (c) | ϕ | Angle between the maximum principal residual stress and gage (a) |
| $\sigma_{1,2}(z)$ | Principal residual stresses | $\varepsilon_x(H)$ | Released strain on the surface |
| H | Groove total depth | E | Elasticity constant |
| Z | Groove depth | $\varepsilon_k(H)$ | Relived strain on the surface |
| n | Number of step | Δl | Average displacement |
| a_{ni} | Influence coefficients | b_{ni} | Influence coefficients |
| L_0 | Gage length of the strain gage | ν | Poisson's ratio |

*Corresponding author: M. Honarpisheh (Assistant Professor)

E-mail address: honarpisheh@kashanu.ac.ir

<http://dx.doi.org/10.22084/jrstan.2019.17330.1069>

ISSN: 2588-2597

| | | | |
|--------------------|--|---------------------|---|
| $A(H, Z)$ | Influence function | $B(H, Z)$ | Influence function |
| θ_i | Angle between the gage (a) and maximum principal residual stress | ε_{an} | Strain in direction of the strain gages (a) and n th step |
| ε_{bn} | Strain in direction of the strain gages (b) and n th step | ε_{cn} | Strain in direction of the strain gages (c) and n th step |
| σ_{ai} | Residual stresses in ith layer along the gages a | σ_{bi} | Residual stresses in ith layer along the gages b |
| σ_{ci} | Residual stresses in ith layer along the gages c | ε_{kni} | Strain in direction of K and n th step and i th condition |

1. Introduction

It is well-known that the residual stresses have significant effects on the mechanical properties and dimensional stability of the components, especially those which are subjected to the cyclic loading. For an experimental analysis of residual stresses, several methods could be used. Generally, the residual stress measurement methods are classified as destructive, semi-destructive, and non-destructive. Mechanical destructive and semi-destructive methods are often used for residual stress analysis, because of their properties such as accuracy of measurement, accessibility, and reasonable costs. Hole drilling [1-3], ring-core [4], deep hole drilling [5], slitting [6-9] and contour [10-12] are famous mechanical residual stress measurement techniques. The ring-core method is used to measure the residual stresses in the surface and subsurface of the components, especially those manufactured by the forging and casting. The ring-core method uses the principal basis of the hole-drilling. In this method a special rosette is bounded on the surface of the component, then an annular groove is removed around it step by step. The released strains due to the material removing are measured by strain rosette. In the next step, the measured strains are used to evaluate the residual stresses. To calculate the non-uniform residual stresses by the ring-core method, two computational techniques named as incremental and integral may be used.

Václavík et al. [13] measured residual stresses in a heavy forged shaft by ring-core and hole drilling methods. It was expressed that the ring-core is a suitable method to measure the subsurface residual stresses. Keil [14] presented the incremental technique and also calculated the calibration coefficients by experimental tension test. Menda et al. [15, 16] used a 3D FE model to study the parameters of the model on the calibration coefficients of the integral technique. They also experimentally measured the residual stresses by the ring-core method. Bouffieux et al. [17] compared the residual stresses on long rolled profiles, measured by X-ray diffraction, ring-core, and the sectioning methods. They expressed that in thin-walled thickness specimen the results of residual stress measurement by three

methods were close. Civín and Vlk [18] studied the condition of loading in the FE analysis of the ring-core method and incremental technique. Moazam and Honarpisheh [19] measured the residual stresses in the rail grade UIC60 by the ring-core and sectioning methods. Valentini et al. [20] presented an automatic system to measure the residual stresses by the ring-core method; the residual stresses were also measured in a forged shaft. Ajovalasit et al. [21] presented the integral method to be used for the ring-coring. Moazam and Honarpisheh [22] presented a set of calibration coefficients to calculate the non-uniform residual stresses by the ring-core incremental technique. Montay et al. [23] presented a 3D FE model to determine the calibration coefficients of the integral technique for the hole drilling method. Barsanti et al. [4] used two plane harmonic elements to calculate the calibration coefficient of the integral method. Zuccarello et al. [24] studied the related uncertainties on non-uniform residual stress measurement by the ring-core. Ghaedamini et al. [25] used the ring-core method to measure the non-uniform residual stresses in the laminated composite. Wern [26] presented a procedure to determine complete stress tensor by the hole drilling and ring-core method. Moharrami and Sadri [27] studied the effect of the plasticity on residual stress measurement by the ring-core method. Wern [28] presented a procedure to calculate the calibration data for the hole drilling and ring-core method. The hole drilling method was standardized by ASTM E837 [29]. This standard, introduced a special procedure to calculate the non-uniform residual stresses based on the Schajer [30] researches about determination of the non-uniform residual stresses by the hole drilling. The calibration coefficients for an isotropic and linear elastic material are presented in the ASTM E837 [29]. However, for non-isotropic materials, composite, in the case that the material is manufactured by several layers, in determining the residual stresses in cladding or covers and other cases which are out of the standard scope, determining the calibration coefficients are mandatory. The ring-core method uses the same basis as the hole drilling, but there is not any standard document which covers the ring core method. Therefore researches in determining the accurate coefficients to calculate the non-uniform residual stresses are still continued.

The aims of this paper are to (i) present an FE model to determine the necessary calibration coefficients for the integral technique and, (ii) compare the accuracy of the two computational techniques: incremental and integral and (iii) measure the surface and subsurface residual stresses in an extruded aluminum ingot grade 7075-T6 by the ring-core method. The novelty of this paper is using the special case of loading to make the shear stresses and also presenting the accurate calibration coefficient and procedure to calculate the non-uniform residual stresses by the ring-core method. The presented calibration coefficients are independent of the elasticity modulus and the Poisson's ratio effects in the range of $0.25 \leq \nu \leq 0.35$.

2. Fundamental of the Ring-core Incremental and Integral Techniques

To determine the residual stresses by the ring-core method, an annular groove was produced around the special strain rosette which was bounded on the surface of the specimen (see Fig. 1). The released strains were recorded and then were used to calculate the residual stresses. There was not standard geometry for the annular groove, but the most of researchers used the geometry similar to those indicated in Fig. 2 [16, 18, 19, 21, 22, 27].

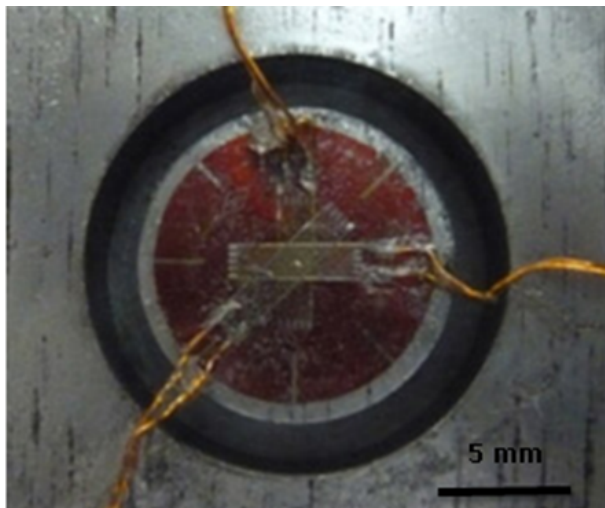


Fig. 1. Typical rosette which uses in the ring-core method.

To calculate the non-uniform residual stresses by the ring-core method, two computational techniques, incremental and integral, could be used. In the incremental strain method, the value of the stresses is calculated in the directions of the rosette strain gages by the equations (1) to (3). In the next step, the principal residual stresses and the angle between maximum principal residual stress and gage (a) are calculated respectively by equations (4) and (5).

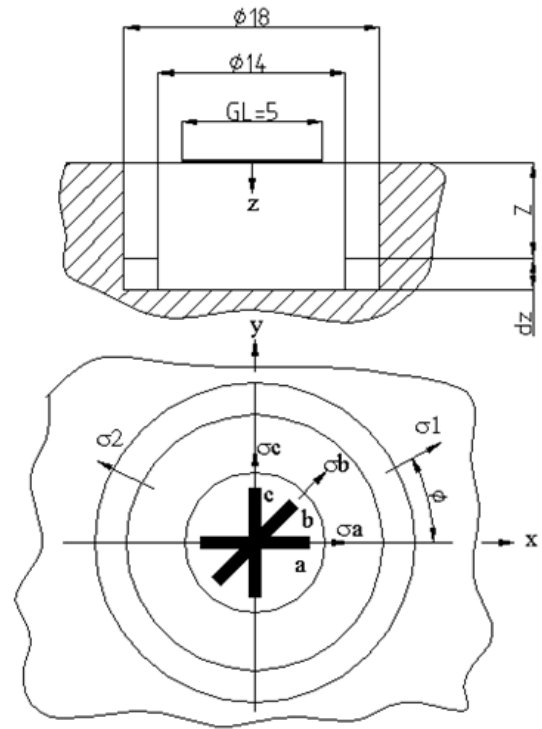


Fig. 2. The geometry and rosette strain gauges configuration using in the ring-core method.

$$\sigma_a(z) = \frac{E}{K_1^2 - \nu^2 K_2^2} \left[K_1(z) \frac{d\varepsilon_a(z)}{dz} + \nu K_2(z) \frac{d\varepsilon_c(z)}{dz} \right] \quad (1)$$

$$\sigma_b(z) = \frac{E}{K_1^2 - \nu^2 K_2^2} \left[K_1(z) \frac{d\varepsilon_b(z)}{dz} + \nu K_2(z) \left(\frac{d\varepsilon_a(z)}{dz} - \frac{d\varepsilon_b(z)}{dz} + \frac{d\varepsilon_c(z)}{dz} \right) \right] \quad (2)$$

$$\sigma_c(z) = \frac{E}{K_1^2 - \nu^2 K_2^2} \left[K_1(z) \frac{d\varepsilon_c(z)}{dz} + \nu K_2(z) \frac{d\varepsilon_a(z)}{dz} \right] \quad (3)$$

$$\sigma_{1,2}(z) = \frac{\sigma_a(z) + \sigma_c(z)}{2} \pm \frac{1}{2} \sqrt{2} \sqrt{[\sigma_b(z) - \sigma_a(z)]^2 + [\sigma_b(z) - \sigma_c(z)]^2} \quad (4)$$

$$\phi = \frac{1}{2} \arctan \frac{2\sigma_b(z) - \sigma_a(z) - \sigma_c(z)}{\sigma_a(z) - \sigma_c(z)} \quad (5)$$

In the equations (1) to (5), $\frac{d\varepsilon_a(z)}{dz}$, $\frac{d\varepsilon_b(z)}{dz}$ and $\frac{d\varepsilon_c(z)}{dz}$ are the released strains due to the depth increment in direction of the strain gages (a), (b) and (c). $K_1(z)$

and $K_2(z)$ is the calibration constant. $\sigma_a(z)$, $\sigma_b(z)$ and $\sigma_c(z)$ are residual stresses in the direction of the gages. $\sigma_{1,2}(z)$ are the principal residual stresses and θ is the angle between the maximum principal residual stress and gage (a). The incremental strain method and necessary calibration coefficients are described in [14, 22].

In the integral technique, the released strain on the surface $\varepsilon_x(H)$ after milling the groove to the depth H is the integral of infinitesimal strains due to the fact that the residual stress $\sigma_x(Z)$ acts on whole groove depth [21].

$$\varepsilon_x(H) = \frac{1}{E} \int_0^H F(H, Z) \sigma_x(z) dz \quad (6)$$

In the Eq. (6), E is the elasticity modulus, $F(H, Z)$ is the function which relates the released strain on the surface to depth Z and total depth H . This kind of formulation was first proposed to be used in the hole-drilling method [30, 31]. In this theory the below assumptions are considered:

- The residual stress field is defined by principal residual stresses σ_1 and σ_2 in the plane parallel to the surface of the component and σ_3 is negligible.
- The gradient of the residual stresses in the measured plane is negligible.
- The material is isotropic and the relaxed strains are elastic.

In evaluation of the residual stresses by ring-core method and integral technique, moreover to the effects of the released strains due to the residual stresses, the variation of the groove geometry due to the depth increment was also considered. Considering Eq. (6) and modifying it to two-dimensional condition, the released strain on the core surface could be expressed by Eq. (7) [31].

$$\varepsilon_k(H) = \frac{1}{E} \int_0^H \left\{ A(H, Z) [\sigma_1(z) + \sigma_2(z)] + B(H, Z) [\sigma_1(z) + \sigma_2(z)] \cos 2 \alpha_k(z) \right\} dz \quad (7)$$

In the Eq. (7), $\varepsilon_k(H)$ is the released strain on the core surface after milling the annular groove to depth (H) , $\sigma_1(z)$ and $\sigma_2(z)$ are the principal residual stresses at depth (Z) , α_k is direction of maximum principal residual stress and measuring direction K ($K = a, b$ and c) and $A(H, Z)$ and $B(H, Z)$ are influence functions. Eq. (7) for n step could be written as Eq. (8).

$$\varepsilon_{kn} = \sum_{i=1}^n \varepsilon_{kni}, \quad k = a, b, c \quad (8)$$

In the Eq. (8), ε_{kni} just depends on the stresses in the i^{th} layer (attention to Fig. 2) and could be expressed as Eq. (9).

$$\varepsilon_{kn} = \frac{a_{ni}}{E} (\sigma_{1i} + \sigma_{2i}) + \frac{b_{ni}}{E} (\sigma_{1i} - \sigma_{2i}) \cos 2 \alpha_{ki}, \quad (9)$$

$k = 1, b, c$

In equation (9), σ_{1i} and σ_{2i} are the principal residual stresses in the i^{th} layer, α_{ki} is the angle between the maximum principal residual stress and measuring direction k , a_{ni} and b_{ni} are influence coefficients and they are related to n^{th} depth increment and i^{th} layer. The ring-core rosette consisted of three strain gage which were oriented at 0, 45 and 90 degree, therefore, the measured strains in each gage could be written as equations (10) to (12).

$$\varepsilon_{an} = \frac{1}{E} \sum_{i=1}^n \left[a_{ni} (\sigma_{1i} + \sigma_{2i}) + \frac{b_{ni}}{E} (\sigma_{1i} - \sigma_{2i}) \cos 2\theta_i \right], \quad k = a, b, c \quad (10)$$

$$\varepsilon_{bn} = \frac{1}{E} \sum_{i=1}^n \left[a_{ni} (\sigma_{1i} + \sigma_{2i}) + \frac{b_{ni}}{E} (\sigma_{1i} - \sigma_{2i}) \sin 2\theta_i \right], \quad k = a, b, c \quad (11)$$

$$\varepsilon_{cn} = \frac{1}{E} \sum_{i=1}^n \left[a_{ni} (\sigma_{1i} + \sigma_{2i}) - \frac{b_{ni}}{E} (\sigma_{1i} - \sigma_{2i}) \cos 2\theta_i \right], \quad k = a, b, c \quad (12)$$

In the equations (10) to (12), θ_i is the angle between the gage (a) and maximum principal residual stress. The start point is from the gage (a) and angle is measured counter-clockwise. It is possible to determine the residual stress field and the direction of the maximum principal stresses by solving the equations (10) to (12). The same procedure was used in the hole-drilling method [30, 31], and it is recommended to separate the hydrostatic and shear stress fields. Therefore the equations (13) to (15) could be written.

$$\varepsilon_{an} + \varepsilon_{cn} = \frac{2}{E} \sum_{i=1}^n a_{ni} (\sigma_{ai} + \sigma_{ci}) \quad (13)$$

$$\varepsilon_{an} - \varepsilon_{cn} = \frac{2}{E} \sum_{i=1}^n b_{ni} (\sigma_{ai} + \sigma_{ci}) \quad (14)$$

$$2\varepsilon_{bn} - \varepsilon_{an} - \varepsilon_{cn} = \frac{2}{E} \sum_{i=1}^n b_{ni} (2\sigma_{bi} - \sigma_{ai} - \sigma_{ci}) \quad (15)$$

In the equations (13) to (15), σ_{ai} , σ_{bi} and σ_{ci} are the residual stresses in i^{th} layer along the gages a , b , and c . The hydrostatic and shear stresses could be written as equations (16) to (18).

$$\sigma_{an} + \sigma_{cn} = \frac{1}{a_{nn}} \left[\frac{2}{E} (\varepsilon_{an} + \varepsilon_{cn}) - \sum_{i=1}^{n-1} a_{ni} (\sigma_{ai} + \sigma_{ci}) \right] \quad (16)$$

$$\sigma_{an} - \sigma_{cn} = \frac{1}{b_{nn}} \left[\frac{2}{E} (\varepsilon_{an} - \varepsilon_{cn}) - \sum_{i=1}^{n-1} b_{ni} (\sigma_{ai} - \sigma_{ci}) \right] \quad (17)$$

$$2\sigma_{bn} - \sigma_{an} - \sigma_{cn} = \frac{1}{b_{nn}} \left[\frac{2}{E} (2\varepsilon_{bn} - \varepsilon_{an} - \varepsilon_{cn}) - \sum_{i=1}^{n-1} b_{ni} (2\sigma_{bi} - \sigma_{ai} - \sigma_{ci}) \right] \quad (18)$$

In the equations (16) to (18) the unknown parameters are σ_{an} , σ_{bn} and σ_{cn} because the ε_{an} , ε_{bn} and ε_{cn} are measured by the strain gages after each depth increment and the calibration coefficients a_{ni} and b_{ni} could be determined by the numerical analysis. When σ_{an} , σ_{bn} and σ_{cn} are determined, the principal residual stresses and their directions could be calculated by equations (4) and (5).

3. Determination of the Calibration Coefficients

It is necessary to determine the calibration coefficients to use the integral method. The calibration coefficients for the hole-drilling are presented by ASTM E837 [29], but there is not any standard document for the ring-core method. The calibration coefficients depend on groove geometry, depth increment, strain rosette dimensions, and Poisson's ratio. The calibration coefficients

could be determined by numerical analysis and considering the equation (9). Unlike the incremental technique, determining the calibration coefficients of the integral technique by experimental test is impossible. In real material the residual stresses are released by cutting the annular groove, but in the numerical analysis process the opposite case is considered and the stresses are applied to the boundaries of the annular groove in each step. The stresses were applied according to Fig. 3 to consider the effect of geometry change due to the released strains on the core surface.

It is possible to determine the coefficients a_{ni} by applying the hydrostatic stress field to the model. Therefore, if $\sigma_1 = \sigma_2$ then, the $\varepsilon_{ani} = \varepsilon_{bni} = \varepsilon_{cni} = \varepsilon_{ni}$ and a_{ni} could be determined by the equation (19).

$$a_{ni} = \frac{E}{2\sigma_1} \varepsilon_{ni} \quad (19)$$

By attention to equation (9), it is possible to calculate the coefficient b_{ni} by considering the $\sigma_1 = -\sigma_2$ and $\alpha_{ki} = 0$. Therefore, equation (20) could be written.

$$b_{ni} = \frac{E}{2\sigma_1} \varepsilon_{ani} \quad (20)$$

Calibration process was performed by finite element analysis in ABAQUS package [32]. The model parameters are indicated in the Table 1 and according to the symmetry only a quarter of the model was considered.

Table 1
Parameters of the finite element model for determining the calibration coefficients.

| Parameters | Value |
|------------------------------------|------------|
| Dimension (mm) | Ø100 × 50 |
| Annular groove (mm) | Ø14-Ø18 |
| Elasticity modulus (GPa) | 200 |
| Yield stress (MPa) | 240 |
| Poisson's ratio | 0.3 |
| Element type | C3D20-C3D8 |
| Gage length of strain rosette (mm) | 5 |

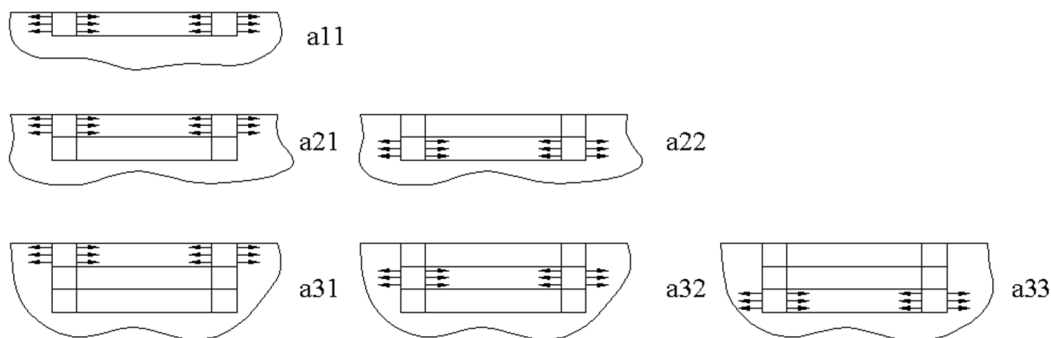


Fig. 3. Loading condition for determination of the calibration coefficients.

The dimensions of the model were very bigger than the strain rosette and the annular groove to avoid the edge effect. The step depth was considered 0.25mm and the total depth of the groove was 5mm. The loading conditions for the determining the calibration coefficients are indicated in Fig. 4. To analyze the process and to determine the calibration coefficients, the total number of single analyses was $2 \times (20 \times (20 + 1)) = 840$.

After the mesh study, mesh size in strain gage position and in the region between the rosette and an annular groove were considered 0.25 and 0.5mm, respectively, and global size of the mesh was 2mm. Fig. 5 indicates the different mesh size in the model.

Study about the type of the elements indicated that

there was no significant difference between the results of using the elements C3D20 and C3D8. While using the element C3D20 needs much more time for calculation. Therefore, the element type C3D8 was used for the FE analyses. Fig. 6 indicates the FE models after 5th step and in depth $H = 1.25\text{mm}$.

The positions of the strain gages were partitioned on the model surface. To calculate the strains after each depth increment, displacement of the nodes along the strain gages was considered. Displacement of the nodes was measured at each step and the strains were calculated by equation (21).

$$\varepsilon_{ni} = \frac{\Delta l}{L_0} \tag{21}$$

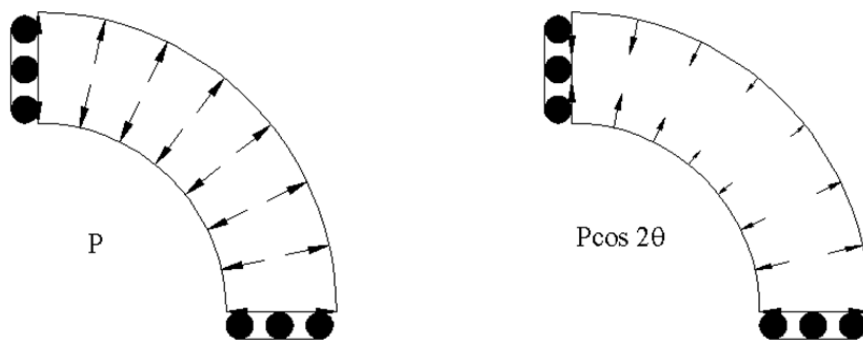


Fig. 4. Hydrostatic and shear loading for determining the calibration coefficients.

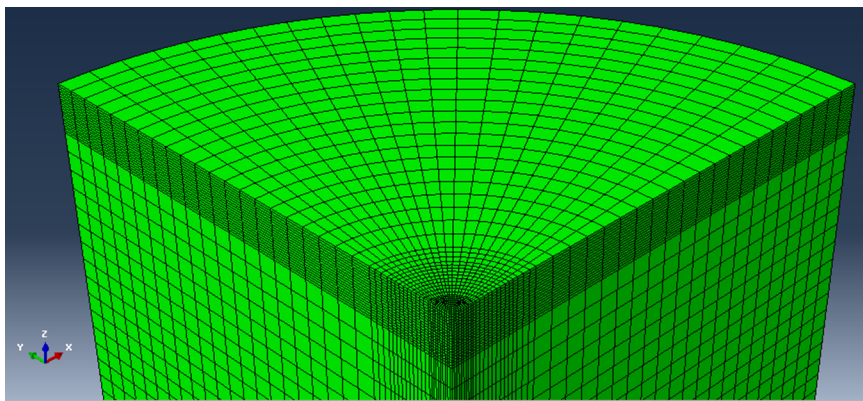


Fig. 5. Mesh size of the FE model.

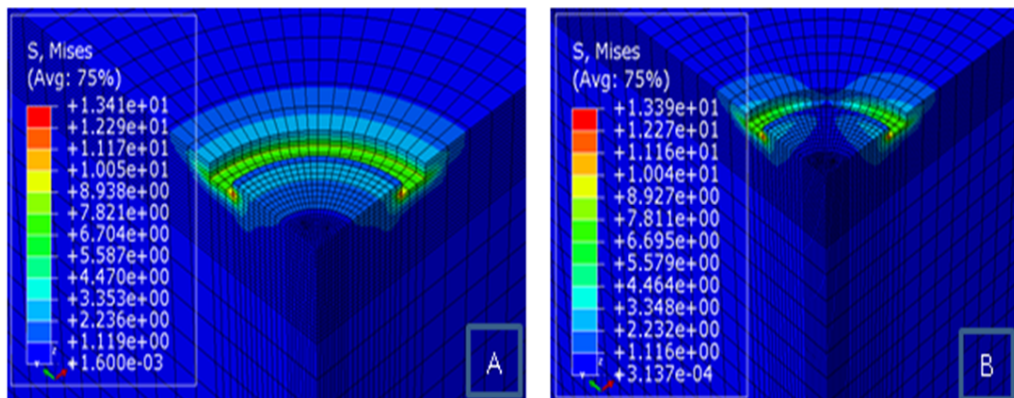


Fig. 6. Model in depth $H = 1.25\text{mm}$, a) Process of determining the a_{ni} and, b) Process of determining the b_{ni} .

In the equation (21), ε_{ni} is the strain in the strain gage direction ($n = a, b$ or c), Δl is the average displacement along the strain gage direction and L_0 is the gage length. After calculating the strains in all of the 840 single models, the calibration coefficients were calculated according to equations (19) and (20) and the results are indicated in the Table 2 and 3.

4. Validation of the Calibration Coefficients

To show the effectiveness of the presented coefficients and also, to compare the results of the integral and incremental techniques, bending process and the ring-core method were analyzed by numerical method. The calculations were performed by ABAQUS finite ele-

ment package [32]. Table 4 indicates the parameters of the model and material behavior was considered as elastic- perfectly plastic. In the first step, appropriate moment was applied to create pure bending in the model. In the second step the load was removed and residual stresses were created, then the ring core method was performed in 20 steps (depth step= 0.25mm).

After the mesh study, the global size of the mesh and mesh size of the rosette portion were respectively considered as 5mm and 0.83mm. Three cases A, B, and C were selected to study the ability of the presented procedure to detect the gradient of residual stresses. The loading condition in each case is indicated in the Table 5. Fig. 7 indicates the model after bending and ring-core processes.

Table 2
 $a_{ni} \times (-1 \times 10^{-5})$ Coefficients-continued.

| Depth (mm) | 0.25 | 0.5 | 0.75 | 1 | 1.25 | 1.5 | 1.75 | 2 | 2.25 | 2.5 |
|------------|------|------|------|------|------|------|------|------|------|------|
| 0.25 | 761 | | | | | | | | | |
| 0.5 | 1268 | 973 | | | | | | | | |
| 0.75 | 1732 | 1492 | 1103 | | | | | | | |
| 1 | 2165 | 1926 | 1631 | 1172 | | | | | | |
| 1.25 | 2556 | 2318 | 2042 | 1700 | 1195 | | | | | |
| 1.5 | 2903 | 2664 | 2400 | 2088 | 1713 | 1180 | | | | |
| 1.75 | 3205 | 2965 | 2707 | 2416 | 2077 | 1680 | 1135 | | | |
| 2 | 3464 | 3224 | 2970 | 2690 | 2375 | 2017 | 1610 | 1067 | | |
| 2.25 | 3683 | 3443 | 3192 | 2919 | 2619 | 2288 | 1920 | 1513 | 984 | |
| 2.5 | 3865 | 3626 | 3377 | 3109 | 2819 | 2504 | 2164 | 1795 | 1396 | 890 |
| 2.75 | 4015 | 3776 | 3529 | 3266 | 2982 | 2678 | 2354 | 2012 | 1650 | 1266 |
| 3 | 4136 | 3899 | 3654 | 3393 | 3114 | 2817 | 2505 | 2179 | 1842 | 1492 |
| 3.25 | 4233 | 3997 | 3753 | 3495 | 3220 | 2928 | 2623 | 2309 | 1987 | 1661 |
| 3.5 | 4310 | 4075 | 3832 | 3576 | 3303 | 3016 | 2717 | 2409 | 2098 | 1786 |
| 3.75 | 4370 | 4136 | 3894 | 3639 | 3369 | 3085 | 2789 | 2487 | 2183 | 1880 |
| 4 | 4416 | 4182 | 3942 | 3688 | 3419 | 3137 | 2845 | 2547 | 2247 | 1951 |
| 4.25 | 4450 | 4217 | 3977 | 3725 | 3457 | 3177 | 2887 | 2592 | 2296 | 2004 |
| 4.5 | 4474 | 4242 | 4004 | 3752 | 3485 | 3206 | 2918 | 2625 | 2331 | 2042 |
| 4.75 | 4492 | 4260 | 4022 | 3771 | 3505 | 3227 | 2940 | 2648 | 2357 | 2070 |
| 5 | 4505 | 4274 | 4036 | 3785 | 3520 | 3242 | 2956 | 2665 | 2375 | 2089 |

Table 2.
Continued.

| Depth (mm) | 2.75 | 3 | 3.25 | 3.5 | 3.75 | 4 | 4.25 | 4.5 | 4.75 | 5 |
|------------|------|------|------|------|------|-----|------|-----|------|----|
| 2.75 | 791 | | | | | | | | | |
| 3 | 1129 | 690 | | | | | | | | |
| 3.25 | 1329 | 991 | 590 | | | | | | | |
| 3.5 | 1475 | 1165 | 856 | 495 | | | | | | |
| 3.75 | 1582 | 1291 | 1006 | 726 | 406 | | | | | |
| 4 | 1662 | 1382 | 1113 | 853 | 604 | 324 | | | | |
| 4.25 | 1720 | 1447 | 1188 | 943 | 710 | 491 | 249 | | | |
| 4.5 | 1762 | 1495 | 1241 | 1004 | 784 | 578 | 388 | 183 | | |
| 4.75 | 1793 | 1528 | 1279 | 1047 | 833 | 637 | 457 | 295 | 125 | |
| 5 | 1814 | 1551 | 1305 | 1076 | 866 | 675 | 503 | 348 | 213 | 76 |

Table 3
 $b_{ni} \times (-1 \times 10^{-5})$ Coefficients-continued.

| Depth (mm) | 0.25 | 0.5 | 0.75 | 1 | 1.25 | 1.5 | 1.75 | 2 | 2.25 | 2.5 |
|------------|------|------|------|------|------|------|------|------|------|------|
| 0.25 | 744 | | | | | | | | | |
| 0.5 | 1263 | 978 | | | | | | | | |
| 0.75 | 1740 | 1518 | 1134 | | | | | | | |
| 1 | 2193 | 1974 | 1694 | 1236 | | | | | | |
| 1.25 | 2615 | 2398 | 2140 | 1811 | 1295 | | | | | |
| 1.5 | 3006 | 2787 | 2542 | 2247 | 1878 | 1322 | | | | |
| 1.75 | 3366 | 3144 | 2905 | 2632 | 2304 | 1905 | 1322 | | | |
| 2 | 3696 | 3471 | 3235 | 2972 | 2671 | 2318 | 1898 | 1299 | | |
| 2.25 | 3997 | 3770 | 3533 | 3276 | 2990 | 2667 | 2295 | 1863 | 1260 | |
| 2.5 | 4270 | 4040 | 3803 | 3549 | 3271 | 2965 | 2625 | 2241 | 1805 | 1206 |
| 2.75 | 4518 | 4284 | 4045 | 3792 | 3519 | 3224 | 2902 | 2552 | 2163 | 1729 |
| 3 | 4740 | 4504 | 4262 | 4009 | 3739 | 3449 | 3139 | 2808 | 2453 | 2066 |
| 3.25 | 4939 | 4700 | 4456 | 4201 | 3932 | 3646 | 3344 | 3024 | 2689 | 2335 |
| 3.5 | 5116 | 4874 | 4627 | 4371 | 4102 | 3818 | 3520 | 3209 | 2886 | 2551 |
| 3.75 | 5273 | 5028 | 4779 | 4521 | 4251 | 3968 | 3672 | 3366 | 3051 | 2729 |
| 4 | 5411 | 5163 | 4912 | 4652 | 4381 | 4097 | 3803 | 3500 | 3191 | 2876 |
| 4.25 | 5532 | 5282 | 5028 | 4766 | 4493 | 4209 | 3916 | 3614 | 3308 | 3000 |
| 4.5 | 5636 | 5383 | 5127 | 4863 | 4589 | 4305 | 4011 | 3711 | 3407 | 3102 |
| 4.75 | 5724 | 5470 | 5212 | 4946 | 4671 | 4385 | 4091 | 3792 | 3489 | 3187 |
| 5 | 5796 | 5540 | 5280 | 5013 | 4737 | 4450 | 4156 | 3857 | 3555 | 3254 |

Table 3.
 Continued.

| Depth (mm) | 2.75 | 3 | 3.25 | 3.5 | 3.75 | 4 | 4.25 | 4.5 | 4.75 | 5 |
|------------|------|------|------|------|------|------|------|------|------|-----|
| 2.75 | 1143 | | | | | | | | | |
| 3 | 1680 | 1073 | | | | | | | | |
| 3.25 | 1954 | 1542 | 999 | | | | | | | |
| 3.5 | 2202 | 1833 | 1438 | 923 | | | | | | |
| 3.75 | 2399 | 2061 | 1707 | 1331 | 846 | | | | | |
| 4 | 2559 | 2239 | 1914 | 1578 | 1224 | 771 | | | | |
| 4.25 | 2691 | 2383 | 2075 | 1766 | 1449 | 1118 | 698 | | | |
| 4.5 | 2799 | 2499 | 2202 | 1910 | 1618 | 1321 | 1014 | 627 | | |
| 4.75 | 2887 | 2592 | 2303 | 2021 | 1744 | 1471 | 1195 | 912 | 560 | |
| 5 | 2957 | 2665 | 2382 | 2106 | 1839 | 1579 | 1324 | 1067 | 807 | 487 |

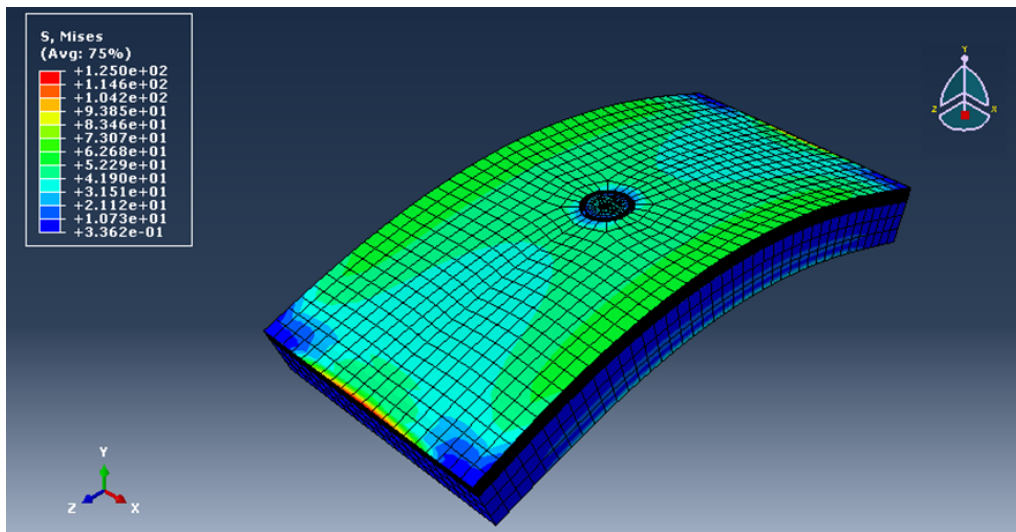


Fig. 7. FEM model in case (C) after bending and ring-core process.

Direction (a) was considered along the largest dimension of the model (200mm). After performing the process, the strain in three directions a, b, and c (see Fig. 2) was measured. The measured strains in different cases are indicated in Fig. 8 to 10.

Table 4
Parameters of the finite element model.

| Parameters | Value |
|------------------------------------|----------------|
| Dimension (mm) | 200 × 100 × 20 |
| Annular groove (mm) | Ø14-Ø18 |
| Elasticity modulus (GPa) | 200 |
| Yield stress (MPa) | 240 |
| Poisson's ratio | 0.3 |
| Element type | C3D20 |
| Gage length of strain rosette (mm) | 5 |

The analytical value of residual stresses were calcu-

lated regarding the geometry and case of loading (Table 4 and 5). To calculate the residual stresses by integral method, the equations (4) and (16) to (19) and also the calibration coefficient, which are indicated in the Table 2 and 3, were used. Furthermore, the residual stresses were calculated by the incremental technique and the calibration coefficient, which is presented in [19]. The outputs of the residual stress calculation are indicated in Fig. 11 to 13.

Table 5
Loading condition in pure bending simulation.

| Case | Moment (N.mm) | Plastic deformation depth (mm) |
|------|---------------|--------------------------------|
| A | 2.20E+06 | 5 |
| B | 1.75E+06 | 1 |
| C | 1.95E+06 | 2.5 |

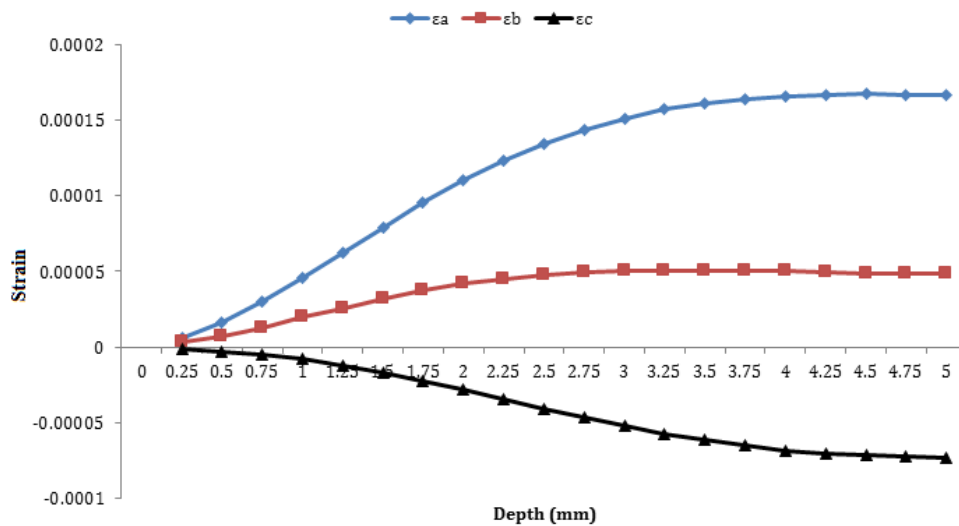


Fig. 8. Measured strains along the strain rosette directions-case A.

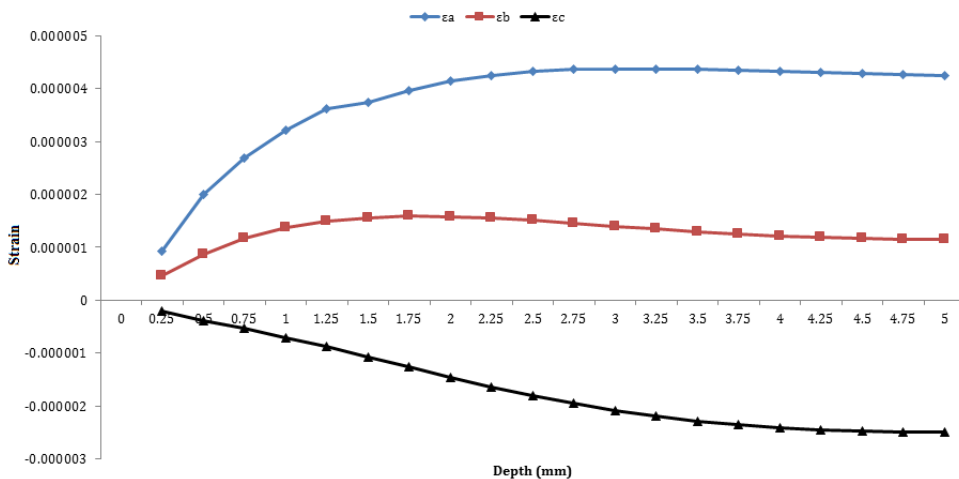


Fig. 9. Measured strains along the strain rosette directions-case B.

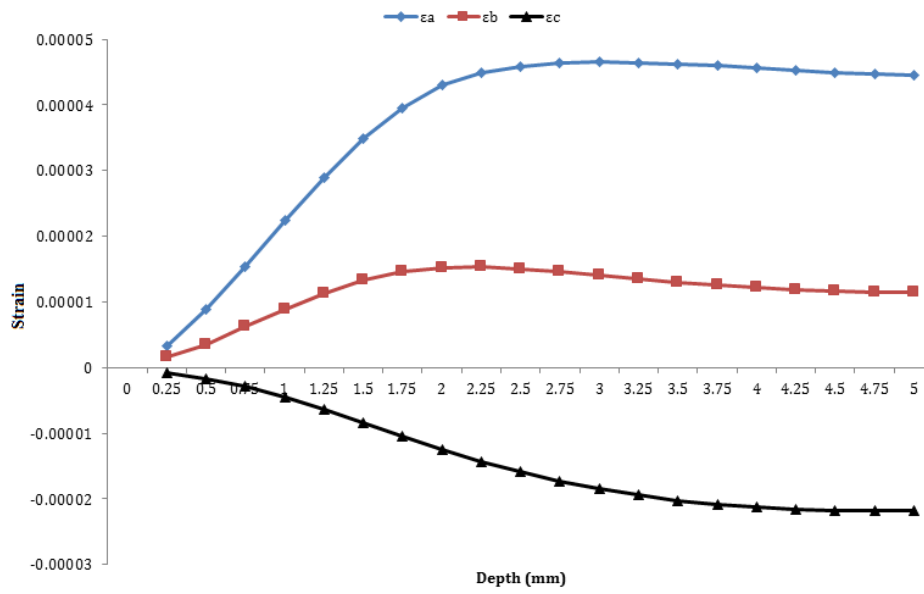


Fig. 10. Measured strains along the strain rosette directions-case C.

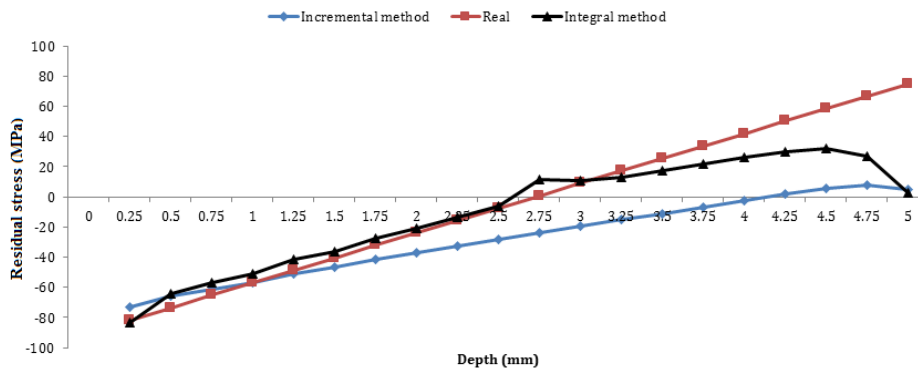


Fig. 11. Calculated maximum residual stresses in pure bending process-case A.

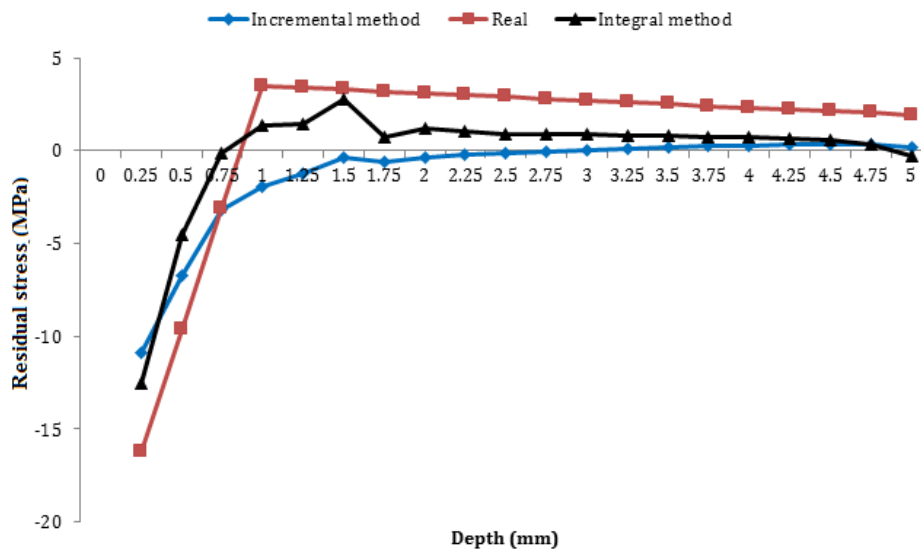


Fig. 12. Calculated maximum residual stresses in pure bending process-case B.

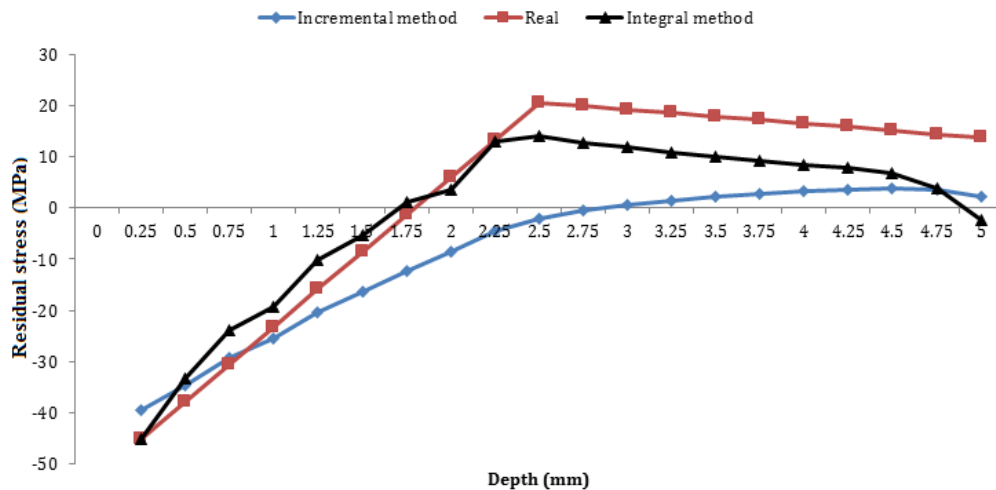


Fig. 13. Calculated maximum residual stresses in pure bending process-case C.

The value of the calculated minimum principal residual stresses and also the angle between the maximum principal residual stress and direction of gage (a) in all cases is almost zero. By comparing the results through Figs. 11 to 13, it is obvious that the integral method predicted the values of the residual stresses very close to the actual value, especially in the near surface depths. The study indicated that the integral method has the ability of detecting the residual stress gradient along the depth. The outputs indicated that the integral method could predict the pattern of the non-uniform residual stresses, but after depth $H = 2.5\text{mm}$ the predicted values diverged from actual ones and maximum error occurred at the depth of $H = 5\text{mm}$.

The incremental method is an approximated computational technique because in this method it is supposed that the released strains in the surface due to the depth increment dz is just dependent on the stresses in the depth increment. In fact the released strains on the core surface not only towered pendent on the stresses in the depth increment, but also the geometry change of the groove affected the measured strains. With respect to the geometry variation of the groove due to the depth increment, the accuracy of the integral technique is more than the incremental method. The results indicated that the ring-core method and integral technique are suitable to measure the surface and sub-surface residual stresses. Accuracy of the ring-core method and integral technique to predict the non-uniform residual stresses along the depth direction is presented in Table 6.

5. Experimental Test

The goal of the test was determining the surface and subsurface residual stresses in an extruded commercial aluminum bar 7075-T6. The precipitation hardening

process could create considerable residual stresses in the specimen. To post-process the material for manufacturing the precise parts, the level of the residual stresses should be considered.

Table 6

Accuracy of the ring-core method and integral technique to detect the non-uniform residual stresses.

| Depth (mm) | Accuracy | Coinciding with the actual value (%) |
|------------|----------|--------------------------------------|
| 0-2.5 | Good | Up to about 95 |
| 2.5-4 | Average | About 75 |
| 4-5 | Weak | - - - |

The sample dimension was selected as $50 \times 50 \times 100\text{mm}$. To measure the surface and subsurface residual stresses the ring-core method and the integral technique were implemented. The strain rosettes TML FR-5-11 [33] were used to measure the released strains during the test. The position of the strain rosette was cleaned with acetone and to bound the strain rosette on the specimen's surface, the CN glue was used according to its manufacturer's instruction [30]. Fig. 14 indicates the specimen and the rosette after milling the annular groove. The test parameters are indicated in the Table 7.



Fig. 14. Specimen after measuring the residual stresses by the ring-core method.

The measured strains are presented in Fig. 15. To calculate the residual stresses, the calibration coefficients were calculated similar to the procedure explained in the previous chapter by changing the elasticity modulus to $E = 70\text{GPa}$. The results were exactly the same as Tables 2 and 3. In fact the presented data in the Tables 2 and 3 are independent of the elasticity modulus and the loading magnitude. Study about the Poisson’s ratio indicated that the calibration coefficients in the range of $0.25 \leq \nu \leq 0.35$ just change the final values about 3 percent. Therefore, using the presented calibration coefficients for this experimental residual stress measurement was logical. The measured

strains and the calculated principal residual stresses by the integral and also incremental techniques are presented in Fig. 15 and 16.

Table 7
Parameters of the experimental ring-core test.

| Parameter | Value |
|--------------------------|--------------------------------|
| Sample dimension (mm) | $50 \times 50 \times 100$ (mm) |
| Sample material | AL 7075 T6 |
| Rosette model | TML FR-5-11 |
| Annular groove dimension | $\text{Ø}14\text{-Ø}18$ (mm) |
| Depth increment | 0.25 (mm) |
| Final depth | 5 (mm) |

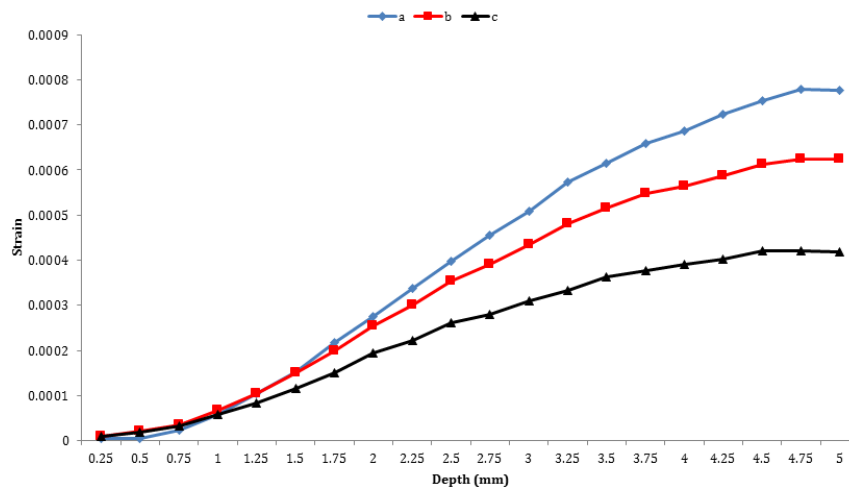


Fig. 15. Measured strains by the ring-core method in the Al 7075T6.

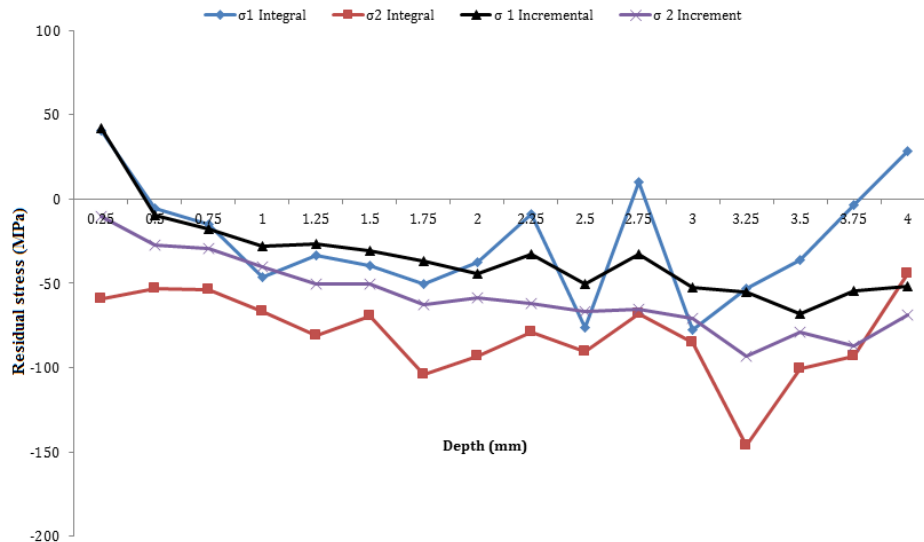


Fig. 16. Calculated principal residual stresses in Al 7075T6 by the ring-core method.

6. Conclusions

Calibration coefficients are pre-required parameters to use the integral computational technique for measuring the non-uniform residual stresses by the ring-core method. In this research, the procedure of determin-

ing the calibration coefficients was studied for the integral technique. Moreover, the ability of the ring-core method to predict the non-uniform residual stresses by two computational methods, namely integral and incremental, were compared. According to the results, it may be concluded that:

- The presented calibration coefficients for the integral technique have enough accuracy to be used in the practical residual stress measurement.
- The calibration coefficients are independent of the elasticity modulus.
- The Poisson's ratio in the range of $0.25 \leq \nu \leq 0.35$ has negligible effect on the calibration coefficients and calculated residual stresses.
- The predicted value of the residual stresses by the integral technique has more accuracy with respect to the incremental method.

References

- [1] M. Sedighi, M. Honarpisheh, Investigation of cold rolling influence on near surface residual stress distribution in explosive welded multilayer, *Strength. Mater.*, 44(6) (2012) 693-698.
- [2] M. Sedighi, M. Honarpisheh, Experimental study of through-depth residual stress in explosive welded Al-Cu-Al multilayer, *Mater. Des.*, 37 (2012) 577-581.
- [3] M. Honarpisheh, V. Zandian, Investigation of residual stresses in stress-relieved samples by heat treatment and ultrasonic methods using hole-drilling method, *Modares Mechanical Engineering*, 14(15) (2015) 273-278.
- [4] M. Barsanti, M. Beghini, C. Santus, A. Benincasa, L. Bertelli, Integral method coefficients for the ring-core technique to evaluate non-uniform residual stresses, *J. Strain Anal. Eng. Des.*, 53(4) (2018) 210-224.
- [5] R. Paynter, A.H. Mahmoudi, M.J. Pavier, D.A. Hills, D. Nowell, C.E. Truman, D.J. Smith, Residual stress measurement by deep hole drilling and trepanning-analysis with distributed dislocations, *J. Strain Anal. Eng. Des.*, 44(1) (2009) 45-54.
- [6] M. Honarpisheh, E. Haghighat, M. Kotobi, Investigation of residual stress and mechanical properties of equal channel angular rolled St12 strips. *Proceedings of the Institution of Mechanical Engineers, Part L: J. Mater. Des. App.*, 232(10) (2018) 841-851.
- [7] M. Kotobi, M. Honarpisheh, Through-depth residual stress measurement of laser bent steel-titanium bimetal sheets, *J. Strain Anal. Eng. Des.*, 53(3) (2018) 130-140.
- [8] M. Kotobi, M. Honarpisheh, Experimental and numerical investigation of through-thickness residual stress of laser-bent Ti samples. *J. Strain Anal. Eng. Des.*, 52(6) (2017) 347-355.
- [9] M. Kotobi, M. Honarpisheh, Uncertainty analysis of residual stresses measured by slitting method in equal-channel angular rolled Al-1060 strips, *J. Strain Anal. Eng. Des.*, 52(2) (2017) 83-92.
- [10] I. Alinaghian, M. Honarpisheh, S. Amini, The influence of bending mode ultrasonic-assisted friction stir welding of Al-6061-T6 alloy on residual stress, welding force and macrostructure, *Int. J. Adv. Manuf. Technol.*, 95(5-8) (2018) 2757-2766.
- [11] I. Alinaghian, S. Amini, M. Honarpisheh, Residual stress, tensile strength, and macrostructure investigations on ultrasonic assisted friction stir welding of AA 6061-T6, *J. Strain Anal. Eng. Des.*, 53 (7) (2018) 494-503.
- [12] M. Honarpisheh, H. Khanlari, A numerical study on the residual stress measurement accuracy using inverse eigenstrain method, *J. Stress. Anal.*, 2(2) (2018) 1-11.
- [13] O. Václavík, P. Weinberg, J. Bohdan, S. Jankovec, S. Holý, Evaluation of residual stresses using ring core method, 14th international conference on experimental mechanics, Poitiers, France, Edited by Fabrice Brémand; *EPJ Web of Conferences*, 6 (2010) id.44004-p.1-6.
- [14] S. Keil, Experimental determination of residual stresses with the ring-core method and an on-line measuring, *Exp. Tech.*, 16(5) (1992) 17-24.
- [15] F. Menda, P. Sarga, F. Trebuna, Estimation of residual stress field uniformity when using the ring-core method, *Adv. Mater. Res.*, 996 (2014) 325-330.
- [16] F. Menda, F. Trebuňa, P. Šarga, Determination of the necessary geometric parameters of the specimen in Ring-Core method, *Appl. Mech. Mater.*, 486 (2014) 90-95.
- [17] C. Bouffioux, R. Pesci, R. Boman, N. Caillet, J. Ponthot, A. Habraken, Comparison of residual stresses on long rolled profiles measured by X-ray diffraction, ring-core and the sectioning methods and simulated by FE method, *Thin Walled Struct.*, 104 (2016) 126-134.
- [18] A. Civ'ın, M. Vlk, Determination of principal residual stresses' directions by incremental strain method, *Appl. Comput. Mech.*, 5 (2011) 5-14.
- [19] M. Moazam, M. Honarpisheh, Residual stresses measurement in UIC 60 rail by ring-core method and sectioning technique, *AUT J. Mech. Eng.*, 2(1) (2018) 99-106.

- [20] E. Valentini, A. Benincasaa, L. Bertelli, An automatic system for measuring residual stresses by the ring-core method, Italian stress analysis association 40th national convention, University of Palermo, (2011).
- [21] A. Ajovalasit, G. Petrucci, B. Zuccarello, Determination of nonuniform residual stresses using the ring-core method, *J. Eng. Mater. Technol.*, 118(2) (1996) 224-228.
- [22] M. Moazam, M. Honarpisheh, Experimental and numerical study on the accuracy residual stress measurement by incremental ring-core method, *AUT J. Mech. Eng.*, 2(2) (2018) 137-148.
- [23] G. Montay, A. Cherouat, J. Lu, N. Baradel, L. Bianchi, Development of the high-precision incremental-step hole-drilling method for the study of residual stress in multi-layer materials: influence of temperature and substrate on ZrO₂-Y₂O₃ 8 wt.% coatings, *Surf. Coat. Technol.*, 155(2-3) (2002) 152-160.
- [24] B. Zuccarello, F. Menda, M. Scafidi, Error and uncertainty analysis of non-uniform residual stress evaluation by using the ring-core method, *Exp. Mech.*, 56(9) (2016) 1531-1546.
- [25] R. Ghaedamini, A. Ghassemi, A. Atrian, Ring-core method in determining the amount of non-uniform residual stress in laminated composites: experimental, finite elements and theoretical evaluation, *A. Arch. Appl. Mech.*, 88(5) (2018) 755-767.
- [26] H. Wern, A new approach to triaxial residual stress evaluation by the hole drilling method, *Strain*, 33(4) (1997) 121-126.
- [27] R. Moharrami, M. Sadri, A procedure for high residual stresses measurement using the ring-core method, *Strain*, 54(4) (2018) 1-11.
- [28] H. Wern, Measurement of non-uniform residual stresses using the hole drilling method, a new integral formalism, *Strain*, 31(2) (1995) 63-68.
- [29] ASTM E837 - 13a. Standard Test Method for Determining Residual Stresses by the Hole-Drilling Strain-Gage Method (2013).
- [30] G.S. Schajer, Measurement of Non-uniform residual stresses using the hole drilling method, *J. Eng. Mater. Technol.*, 110(4) (1988) 338-343.
- [31] G.S. Schajer, Measurement of non-uniform residual stresses using the hole drilling method. Part II: practical application of the integral method, *J. Eng. Mater. Technol.*, 110(4) (1988) 344-349.
- [32] ABAQUS Analysis Users Manual, Version 6.14-2 (2014) Dassault Systems Simulia Corp. RI, USA.
- [33] Tokyo Sokki Kenkyujo Co, Ltd., TML Strain gage catalogue, <http://www.tml.jp/e>.